TU Delft

Delft University of Technology

Stability analysis of thermodiffusively unstable counterflow lean premixed hydrogen flames

Porcarelli, Alessandro; Lapenna, Pasquale Eduardo; Creta, Francesco; Langella, Ivan

DOI
10.1016/j.proci.2025.105906

Publication date
2025

Document Version
Final published version

Published in
Proceedings of the Combustion Institute

Citation (APA)
Porcarelli, A., Lapenna, P. E., Creta, F., & Langella, I. (2025). Stability analysis of thermodiffusively unstable counterflow lean premixed hydrogen flames. *Proceedings of the Combustion Institute*, *41*, Article 105906. https://doi.org/10.1016/j.proci.2025.105906

Important note
To cite this publication, please use the final published version (if applicable).
Please check the document version above.

Copyright
Other than for strictly personal use, it is not permitted to download, forward or distribute the text or part of it, without the consent of the author(s) and/or copyright holder(s), unless the work is under an open content license such as Creative Commons.

Takedown policy
Please contact us and provide details if you believe this document breaches copyrights.
We will remove access to the work immediately and investigate your claim.

This work is downloaded from Delft University of Technology.
For technical reasons the number of authors shown on this cover page is limited to a maximum of 10.

Proceedings of the Combustion Institute 41 (2025) 105906

Contents lists available at ScienceDirect

Proceedings of the Combustion Institute

journal homepage: www.elsevier.com/locate/proci

Stability analysis of thermodiffusively unstable counterflow lean premixed hydrogen flames

Alessandro Porcarelli [a,*], Pasquale Eduardo Lapenna [b], Francesco Creta [b], Ivan Langella [a]

[a] Faculty of Aerospace Engineering, TU Delft, Kluyverweg 1, 2629HS, Delft, Netherlands
[b] Department of Mechanical and Aerospace Engineering, Sapienza, University of Rome, Via Eudossiana 18, 00189, Rome, Italy

ARTICLE INFO

Keywords:
Hydrogen premixed flames
Thermodiffusive instabilities
Strain
Counterflow

ABSTRACT

This study investigates the effect of increasing strain rate on thermodiffusively unstable, lean premixed hydrogen flames in a 2D counterflow configuration through detailed-chemistry numerical simulations for the first time. The analysis of transient flame dynamics without imposed perturbations reveals that a steady-state flame front is achieved only when the strain rate exceeds a certain threshold. Below this threshold, the curved flame tips exhibit an unstable sequential onset and suppression pattern. When subjected to a range of perturbation wavelengths, the flame front exhibits an exponentially increasing wavelength over time, driven by the flame-tangential velocity component, with the applied strain rate acting as the amplification factor. It is shown that any perturbation is damped at sufficiently high applied strain rate conditions after a transient phase. At these high strain regimes, the growth rate transient follows a characteristic onset that depends uniquely on the initial perturbation wavelength and exhibits a linear dependence on the applied strain rate.

1. Introduction

Hydrogen has emerged as a key contributor in addressing climate change, as it offers a zero-carbon alternative to hard-to-electrify sectors like transportation. Recent research efforts have focused on studying hydrogen combustion in lean premixed conditions, where the lower adiabatic flame temperature enables a significant reduction in harmful NO_x emissions. In fact, hydrogen's high reactivity makes it well-suited for achieving ultra-lean regimes without incurring in lean blow-off [1]. However, lean hydrogen flames are also characterised by a very high flame speed, auto-ignition phenomena and growth of thermodiffusive instabilities [2], making flame control and flashback prevention particularly challenging.

Well-established theoretical studies of flame intrinsic instabilities (hydrodynamic and thermodiffusive) are available in literature describing their onset and growth rate at each scale (so-called "dispersion relation") in freely propagating premixed flame configuration using the hydrodynamic model [3], which assumes infinitely thin flame fronts. More simplified theoretical models exist, which under the constant density flow assumption are able to account for lower-than-unity mixture Lewis numbers [4]. Additionally, by incorporating all diffusion effects within a flame speed relation, Creta and Matalon [5] explicitly included strain effects in their model.

Since the recent hit of hydrogen combustion, extensive numerical studies of thermodiffusively unstable flames based on comprehensive modelling have been published [6–8]. Along with high-fidelity simulations, recent works attempted to model thermodiffusive instabilities at sub-filter scales of laminar flames with tabulated chemistry to aid the development of low-fidelity models and design practical combustor settings where lean premixed hydrogen flames are stabilised and controlled [9,10]. Direct numerical simulations [11] and experiments [12] in turbulent conditions further suggested that thermodiffusive instabilities feature a synergistic interaction with turbulence in enhancing hydrogen reactivity and consumption speed, posing further challenges to the accurate modelling of this phenomenon in a large-eddy simulation framework.

While flame instabilities for unstretched freely propagating premixed flames have been investigated by numerous numerical and analytical studies, their onset in strained configurations is less understood. Previous works have shown that hydrogen exhibits a distinctive response to strain, characterised by enhanced overall flame reactivity [13], significant delays in the extinction strain rate [1], reduction in NO_x emissions [14], and mitigation of preferential diffusion effects [15]. Interestingly, a recent work found that increasing strain due to higher Karlovitz number (and thus shear-driven turbulence) in turbulent conditions leads to less recognisable patterns of thermodiffusive instabilities [16], potentially suggesting that any perturbation due to turbulence may be suppressed by stronger tangential velocity gradients.

* Corresponding author.
E-mail address: a.porcarelli@tudelft.nl (A. Porcarelli).

https://doi.org/10.1016/j.proci.2025.105906
Received 15 July 2025; Accepted 1 October 2025
Available online 10 October 2025
1540-7489/© 2025 The Author(s). Published by Elsevier Inc. on behalf of The Combustion Institute. This is an open access article under the CC BY license (http://creativecommons.org/licenses/by/4.0/).

The stability of stagnation-point flames has been only theoretically studied by Sivashinsky et al. [17], highlighting that a sufficiently high strain rate may lead to an overall stabilisation of the perturbation modes in all directions. However, stability analyses based on high-fidelity simulations in strained configurations are still to be done, and it has yet to be demonstrated that strain can by itself suppress intrinsic instabilities, thereby aiding the stabilisation of hydrogen flames.

The purpose of this study is to characterise the response of a lean premixed and strained hydrogen flame front to a range of perturbation wavelengths. Numerical simulations with detailed-chemistry accounting for the relevant transport phenomena in hydrogen flames are performed in 2D laminar counterflow configurations with varying levels of applied strain rate. In this study, we focus on laminar conditions and different fixed applied strain rate as a first step to understand whether thermodiffusively unstable hydrogen flames can be stabilised through strained configurations in practical combustion systems.

2. Computational setup

2.1. Governing equations

Detailed-chemistry, two-dimensional, laminar reacting flow simulations are performed using an *in-house* version of reactingFoam. This transient compressible solver in OpenFOAM has been modified to incorporate mixture-averaged transport and temperature-dependent thermodynamic and transport properties. The reacting Navier–Stokes equations [18] are solved for mass, momentum, sensible enthalpy h and the mass fraction Y_k of $N-1$ species k. In Einstein's notation, the equation for the generic species k is

$$\frac{\partial(\rho Y_k)}{\partial t}+\frac{\partial(\rho u_i Y_k)}{\partial x_i}=-\frac{\partial(\rho V_{k,i} Y_k)}{\partial x_i}+W_k\dot{\omega}_k, \tag{1}$$

where ρ is the mixture density, $V_{k,i}$ is the diffusion velocity of species k, $\dot{\omega}_k$ is the molar rate of production of species k, W_k is the molar mass of species k, and subscripts i and j denote the spatial directions. The mass fraction of the N$^{\text{th}}$ species is found as $Y_N = 1-\sum_{k=1}^{N-1} Y_k$. Body forces, viscous dissipation, and pressure gradients are neglected. The low-Mach ideal gas law and the caloric equation of state are used as thermodynamic model, where in the latter the species heat capacities are obtained using the JANAF polynomials. The species viscosities are calculated *a priori* in Chem1D [19] following the standard kinetic theory [20], and are then tabulated as a logarithmic third-order polynomial function of temperature.

A mixture-averaged diffusion model [18] with velocity correction is used to model the diffusion velocity and account for lean hydrogen's preferential and differential diffusion effects:

$$V_{k,i}=-\frac{D_k^M}{Y_k}\frac{\partial Y_k}{\partial x_i}+V_{c,i}, \tag{2a}$$

$$D_k^M=\frac{1-Y_k}{\sum_{l,k\neq l}^{N} X_l/D_{kl}} \tag{2b}$$

where D_k^M are the mixture-averaged diffusion coefficients and $V_{c,i}$ is the correction velocity:

$$V_{c,i}=\sum_{k=1}^{N} D_k^M\frac{\partial Y_k}{\partial x_i}. \tag{3}$$

Note that the variations of mixture molar mass are relatively small in the present context, therefore the additional term related to the gradients of mixture molar mass in Eq. (2a) has been omitted for simplicity. The correction velocity follows from the mass conservation to ensure that $\sum_{k=1}^{N} j_k = \sum_{k=1}^{N}\rho V_{k,i}Y_k = 0$, where j_k are the species mass fluxes. It is worth noting that, while previous works pointed out that quantitative results may improve by using a multi-component diffusion model [21,22], simplified models like the mixture-averaged used in the present work are commonly used for stability analyses and have been shown not to affect the generalities of the conclusions [6–8,23]. The binary diffusion coefficients D_{kl} in Eq. (2) are computed using the approximation of Hirschfelder et al. [20] and tabulated in OpenFOAM as a function of temperature [24]. The effect of Soret or thermal diffusion is neglected at this stage to reduce computational cost. Despite this assumption might impact the quantitative predictions of perturbation growth rates, the patterns of intrinsic flame instabilities analysed in this work are not affected by this modelling choice [6].

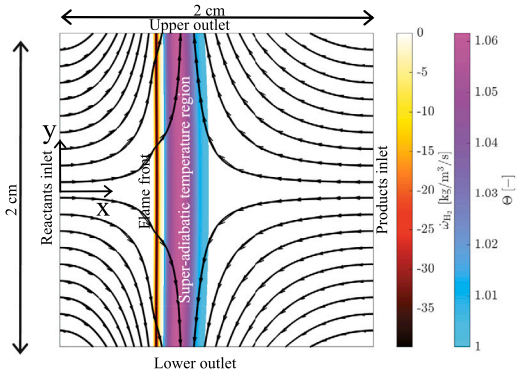

Fig. 1. Sketch of the two-dimensional laminar reactants-to-products counterflow setup, showing the flame solution of case a1000. The flame front is identified by the contour of hydrogen source term $\dot{\omega}_{H_2}$, and super-adiabatic temperatures are visible in the region of super-unity temperature progress variable $\Theta=\frac{T-T_r}{T_p-T_r}$.

The heat flux is found as the composition of conductive and diffusive contributions

$$q_i=q_{i,\text{cond}}+q_{i,\text{diff}}=-\lambda\frac{\partial T}{\partial x_i}+\rho\sum_{k=1}^{N} h_k Y_k V_{k,i}, \tag{4}$$

where mass conservation is ensured by the condition $\sum j_k = 0$, leading to the following expression of the diffusive heat flux

$$q_{i,\text{diff}}=\rho\sum_{k=1}^{N} h_k Y_k V_{k,i}= \rho\sum_{k=1}^{N-1} h_k Y_k V_{k,i}-\rho h_N\sum_{k=1}^{N-1} Y_k V_{k,i}. \tag{5}$$

Similarly to the species viscosities, the species conductivities are also determined *a priori* and tabulated as function of temperature. Radiation and Dufour effects are neglected in this study. Detailed kinetic data of reactions and species transport are taken from the Conaire chemical mechanism [25].

2.2. Computational setup and numerical details

The flame setup consists of a counter-flow reactants-to-products configuration as shown in Fig. 1. As discussed in a recent study [14], such configuration is considered the most suitable to analyse lean premixed hydrogen flames at intensive strain rates. For more details on the setup boundary conditions, the reader is referred to Sec. 1 of the Supplementary Material. Similarly to previous studies performing linear stability analyses of unstretched thermodiffusively unstable flames [6–8], lean conditions are established at an equivalence ratio $\phi = 0.5$ and the reactants temperature and pressure are fixed respectively to $T_r = 300$ K and $p = 1$ atm. At the products boundary, the temperature is prescribed to adiabatic conditions, $T_p = 1646$ K, and the mixture composition is imposed from complete combustion. The nominal applied strain rate in this study is defined as

$$a=\frac{|u_r|+|u_p|}{L}, \tag{6}$$

Table 1
Overview of the four simulations investigated in the present work.

Case name	a [s^{-1}]	s_c [m/s]	δ_f [mm]	τ_f [ms]
a500	331.3	0.596	0.402	0.675
a1000	706.85	0.659	0.371	0.563
a2000	1447.5	0.732	0.346	0.472
a5000	3633.5	0.831	0.299	0.360

where $L = 2$ cm is the domain length, and u_r and u_p are the velocities at the reactants and products boundary, respectively. Four cases at different applied strain rate are investigated in the present study and reported in Table 1 along with their consumption speed s_c, thermal flame thickness $\delta_f = \frac{T_p - T_r}{|\partial T/\partial x|_{\max}}$, and the chemical time scale $\tau_f = \delta_f / s_c$. Different nominal strain rates are achieved by prescribing the velocity at the reactants and products boundary, which are reported in Sec. 1 of the Supplementary Material.

The computations are performed with an implicit second-order Crank–Nicolson discretisation scheme for time marching, combined with a third-order cubic scheme for the convective term of all resolved quantities. A constant time-step is chosen to ensure a maximum CFL number below 0.2. The simulations are first run over a long transient (up to $t = 50\tau_f$) from ignition to a basic steady state (if achieved, see the next section). Then, a single-wavelength perturbation is applied to the flame front at steady state and is tracked until the crests exit the domain in the upper outlet, corresponding to a physical time of up to $t = 7\tau_f$. The domain for all simulations is discretised using a uniform mesh of 800 × 800 finite volumes, resulting in a cell spacing $\Delta x = 2.5 \cdot 10^{-5}$ m. This mesh enables a resolution of the flame structure comparable to prior studies [6], with $n_f = \delta_f / \Delta x$ ranging between 12 and 15.

3. Results and discussion

3.1. Validation

Results obtained using the presented methodology in OpenFOAM were preliminarily validated for a one-dimensional freely propagating premixed hydrogen laminar flame at equivalence ratio $\phi = 0.5$, against those obtained from the well-known code Chem1D [19]. Results indicated a maximum difference of 2.4%, 4.5%, and 5.7% respectively for the mixture fraction dip across the domain, flame thickness, and consumption speed. For further details on this preliminary validation over the 1D setup, the reader is referred to Sec. 2 in the Supplementary Material.

In order to assess the solver's capability in performing stability analyses in thermodiffusively unstable flames, a two-dimensional laminar, freely propagating premixed flame with hydrogen fuel at an equivalence ratio of $\phi = 0.5$ is further simulated on a mesh ensuring 25 cells within the laminar flame thickness. The flame is perturbed with a multi-wavelength perturbation with initial amplitude $A_0 = 0.02\delta_f$, and the dispersion relation in the linear regime is reconstructed following the polychromatic methodology in Al Kassar et al. [8]. Results are reported in Fig. 2, and compared to those in the literature for the same burning regime [6–8]. As observed, the dispersion relation obtained in OpenFOAM is within the range expected from the other literature studies, indicating that the methodology used in the present work is suitable to study thermodiffusively unstable flames.

3.2. Flame dynamics without imposed perturbations

The flame dynamics at different applied strain rates without imposing any perturbation yet is discussed first to have a base reference. At the lowest strain rate, case a500 of Table 1, the flame front does not reach any steady state after an initial transient. As shown in Fig. 3, the flame front is curved and its tips feature a small-amplitude, undamped

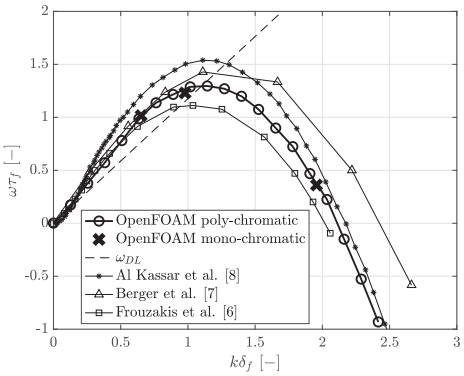

Fig. 2. Dispersion relation for a freely propagating hydrogen flame obtained from the current results, and compared to data from the literature.

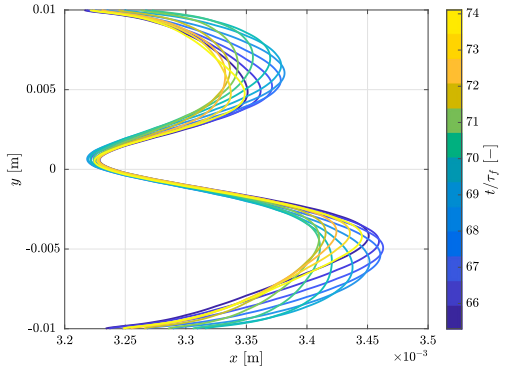

Fig. 3. Low strain rate case a500. Evolution of the flame front as a function of time. Note the different x- and y-axis scales.

sequential onset and suppression pattern in time. This unsteady sequential pattern can be further observed in Fig. 4, showing the variation in time of the flame position (reported only at the lower boundary for simplicity). This unstable sequential pattern is not observed for the other strain rate cases, where after a numerical transient the flame achieves a steady shape in time, which is reported in Fig. 5. Note that, although a steady state is reached for those cases, their respective flame fronts exhibit a mild curvature (observe that the axes in the figure are not uniform). This is however due to some variation in the velocity field near the outlet boundaries, rather than being an intrinsic effect of the flame dynamics. On the contrary, the unsteady a500 case shows an opposite concavity with respect to the other cases. Here, the instantaneous, positively curved flame front $\kappa > 0$ (concave towards the products) near the domain centreline is located more upstream than for the higher strain rate cases at any time, implying that the flame is propagating locally at a higher speed. Conversely, the negatively curved flame fronts $\kappa < 0$ (concave towards the reactants) at $y \approx \pm 5$ mm are located more downstream at any time step as compared to the higher strain rate cases, indicating that the flame speed is slower at these locations. These differences for the a500 case with respect to the cases at higher strain rate are the result of the occurrence of intrinsic instabilities. However, this behaviour is different from that of an unstrained thermodiffusively unstable case, where the flame fingers would keep developing in time, and which is not expected to exhibit the sequential onset and suppression pattern highlighted in Figs. 3 and 4. Indeed, the aforementioned sequential pattern is a characteristic feature of the counterflow configuration, where the velocity at the reactants side decreases (about linearly) in the streamwise direction. This implies that when a positively (negatively) curved flame front, due to its higher (lower) flame speed, propagates upstream (downstream) towards the

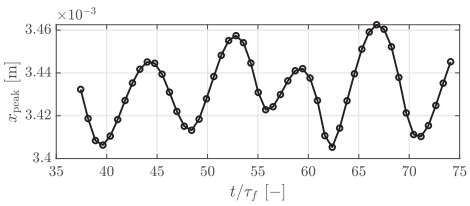

Fig. 4. Low strain rate case a500. Evolution of the x position of the lower flame tip as a function of time.

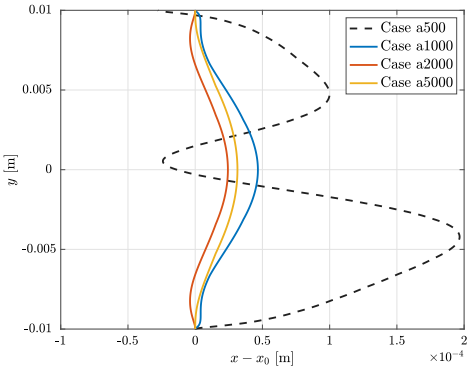

Fig. 5. Steady flame front shape achieved at moderate to high strain rate cases (case a1000 to a5000, solid lines). Comparison to an instantaneous unsteady flame front at low strain rate (case a500, dashed line). Note the different x and y axis scale.

Table 2
Perturbations applied to the basic state flame for cases a1000, a2000 and a5000. λ_0 is the initial perturbation wavelength, k_0 is the corresponding wave number and δ_f is the unstretched flame thickness.

λ_0 [mm]	k_0 [1/mm]	$k_0\delta_f$ [−]
0.65	9.67	3.91
1.3	4.83	1.96
2.6	2.42	0.978
3.9	1.61	0.652
5.2	1.21	0.489
6.5	0.967	0.391

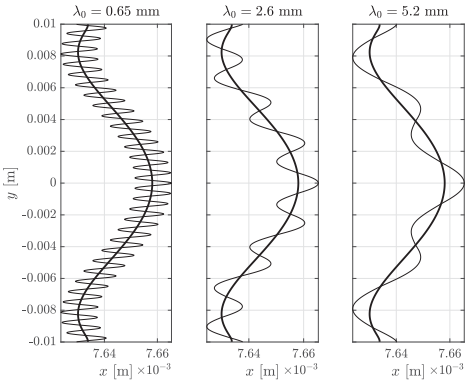

Fig. 6. Basic state flame front (thick line) vs. perturbed flame front (thin line) at different perturbation wavelengths λ_0 for case a2000 of Table 1.

reactants (products), it will also encounter a higher (lower) velocity and lower tangential strain, both counteracting the propagation effect of increased (decreased) flame speed. For this case, the intrinsic instability onset and the stabilising effect of the counterflow configuration are of similar magnitude, so that the unsteady sequential pattern described earlier is achieved. For the higher strain rate cases the velocity gradient in the streamline direction is stronger, implying that the stabilising effect is dominant over the onset of intrinsic instabilities, thus a steady flame front is achieved.

The above results suggest that for sufficiently high strain levels the counterflow configuration stabilises hydrogen flames that would be thermodiffusively unstable in unstretched conditions. This point will be further discussed in the following sections.

3.3. Perturbed flame front dynamics

The steady flame front obtained for cases a1000, a2000, and a5000 of Table 1 discussed in the previous section was perturbed with a single-wavelength or monochromatic signal, and the response of the flame to this perturbation is discussed here. The initial range of perturbation wavelength λ_0 is chosen such that the corresponding wave number $k_0 = 2\pi/\lambda_0$ falls within the unstable modes in the dispersion relation of unstretched flames for the conditions investigated (see Fig. 2). For completeness, one case ($\lambda_0 = 0.65$ mm) is also chosen in the negative growth rate dispersion relation region. The applied perturbations are summarised in Table 2. The normalised wave number $k_0\delta_f$ is also reported as a mean of comparison to the dispersion relation for freely propagating flame in Fig. 2. The perturbation signal is given to all fields with a cosine function to preserve the flame front symmetry, with an initial amplitude of $A_0 = 0.02\delta_f$ (similar to previous studies [7]). An example of how the steady state flame front (basic state) is perturbed in the chosen range of λ_0 is given in Fig. 6. Once the flame is perturbed, as one would expect the initial (imposed) wavelength increases in time due to the effect of the velocity along the y-direction of the counterflow domain (see Fig. 1), which is responsible for flame tangential strain. To better visualise this phenomenon, the reader is referred to Sec. 3 of the Supplementary Material.

Before discussing the evolution in time of λ, it is however convenient to derive an analytical formulation for its expected shape function. Considering that $A_0 \ll \delta_f$, the local tangential strain rate K_s for the opposed-jet configuration can be reduced to that of a flat flame front, $K_s = \frac{\partial u_y}{\partial y}$. Let us also assume that K_s is about constant in time along the flame front during its evolution post-perturbation, which is confirmed by the numerical results (see Sec. 4 in the Supplementary Material). By replacing $y = \lambda/2$ and recalling that $u_y \simeq \frac{dy}{dt} = y'$ for small perturbations, one then obtains

$$\lambda(t) = \lambda_0 e^{K_s t}, \tag{7}$$

and in terms of wave number

$$k(t) = k_0 e^{-K_s t}. \tag{8}$$

In order to compare this solution with the simulation data, an estimate of the exponential factor K_s is necessary. By noting that $K_s = \frac{d(\log(\lambda/\lambda_0))}{dt}$ and recalling that $K_s \approx const$ in time, the exponential factor is obtained by linear interpolation of the function $\log\frac{\lambda(t)}{\lambda_0}$ obtained from the simulations. A comparison between the analytical Eq. (7) with fitted K_s and the simulation data for $\lambda(t)$ is shown in Fig. 7(a). One can observe a very close agreement between the pseudo-analytical expression and the simulation data, implying the assumptions used for the analytical derivation hold. It is worth to note that K_s is directly proportional to the applied strain rate a. In fact

$$\log k(t) = \log k_0 - K_s t \Rightarrow \log(k/k_0) = -K_s t, \tag{9}$$

and thus $\log\frac{k}{k_0}$ as a function of $(K_s t)$ is a straight line with slope -1 for all the investigated cases. Should K_s be directly proportional to a, the same straight line would be obtained when plotting $\log\frac{k}{k_0}$ as a function of (at). This is confirmed with very good approximation by the plot in Fig. 7(b). This aspect is important as it demonstrates that the monochromatically perturbed flame front in a counterflow configuration yields an exponentially increasing wavelength in time

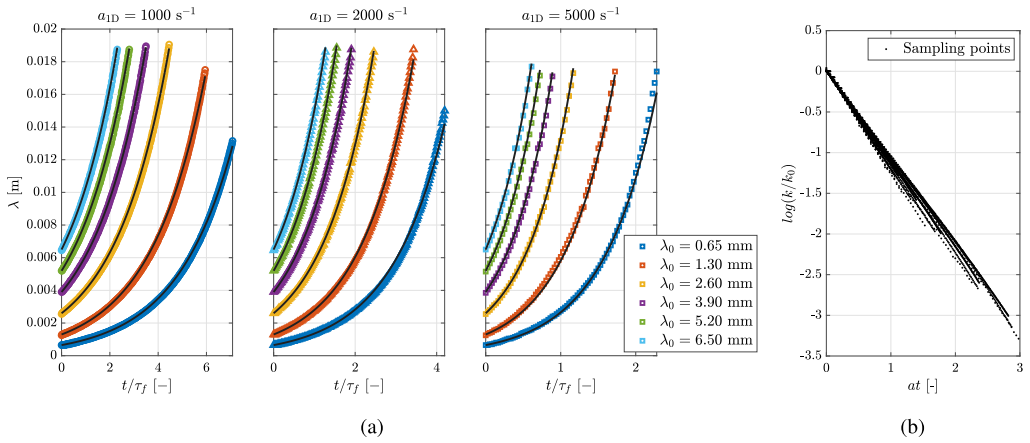

Fig. 7. (a) Comparison between the numerical values of wavelength λ and the pseudo-analytical expression $\lambda = \lambda_0 e^{K_s t}$ for different perturbation wavelengths λ_0 and strain rates. (b) Collapsing sampling points in $at - \log(k/k_0)$ space at all perturbation wave lengths λ_0 and strain rates investigated.

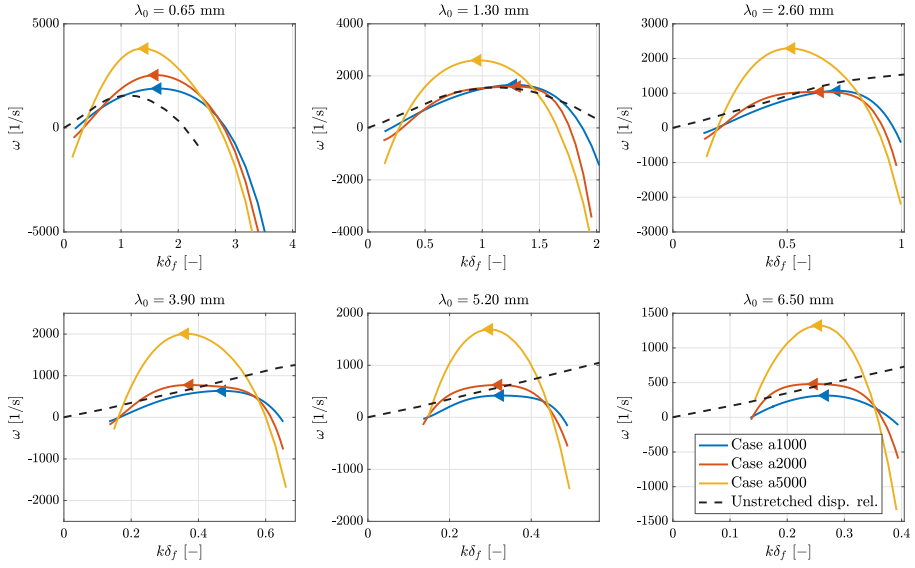

Fig. 8. Growth rate ω as a function of the non-dimensional wave number $k\delta_f$ at different strain rates and different initial perturbation wavelengths λ_0. δ_f is the unstretched laminar flame thickness.

with applied strain rate as amplification factor. Some deviations from the pseudo-analytical expression are found because the local K_s shows moderate variations depending on the local perturbations, which are locally affecting the flow field on the small scales. Yet, the fit remains linear with very good approximation if the global applied strain rate is considered. Note that this exponential wavelength growth found in this simplified laminar case should be considered as fundamental knowledge to analyse the effect of strain on thermodiffusive instabilities. Indeed, in turbulent settings, shear-driven turbulence can establish local random tangential velocity gradients tangential to the flame front, thus significantly altering the instantaneous local strain rate experienced by the flame. In such conditions, we should not expect an exponential growth of λ.

3.4. Perturbation growth rate

The behaviour of the perturbation growth rate ω is investigated in this section for the three stable cases of Table 1 (a1000 to a5000). The growth rate is defined as:

$$\omega = \frac{d(\log A)}{dt} = \frac{1}{A}\frac{dA}{dt}, \tag{10}$$

where A is the time-evolving amplitude. Growth rates are shown for different initial wavelengths and applied strain rates in Fig. 8 as a function of the wave number. The dispersion relation for the unstretched case is also reported for comparison purposes (dashed lines). Note that in order to suppress some noise from the simulation data, the counterflow curves in the figure have been smoothed out using a fifth-order polynomial fit over the sampling points, which are the same as shown in Fig. 7(a) (one every 0.01 ms). The lowest value of k on the x-axis in the plots represents the computed wavelength at the time the last remaining crest reaches the upper outlet of the domain. It is worth mentioning that these plots do not display a dispersion relation. An unstretched premixed flame under a similar monochromatic perturbation exhibits a constant wave number over time in the initial linear regime, corresponding to a constant growth rate and thus enabling the construction of a dispersion relation. However, in strained configurations, k decreases in time according to Eq. (8). Consequently, ω is also not constant for a given λ_0, as no initial linear regime can be identified due to this mode shift. Note that this is also why a fourth-order polynomial, which is generally used to fit a dispersion relation curve [7] following theoretical findings [4], did not provide here a good fit for $\omega(k)$.

For all cases, similar growth rate patterns can be recognised: ω initially exhibits negative values for high values of k (recall that in

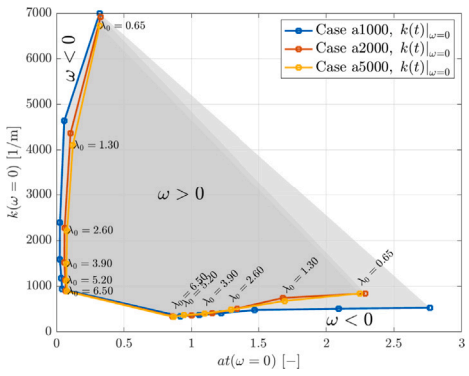

Fig. 9. Isolines of growth rate $\omega = 0$ in the $at - k$ space for different strain rates and initial perturbation wavelengths λ_0 [mm]. The set of points on the left-hand-side of the figure represent the 'earlier' roots of $\omega(k)$ (refer to the roots on the right of $\omega(k)$ in Fig. 8), while the set of points on the bottom-right side represent the 'later' roots (refer to the roots on the left of $\omega(k)$ in Fig. 8).

time the graph should be read from right to left) and increases with (decreasing) k until it becomes positive and reaches a maximum for a certain value k^*. For lower values of k, i.e. further progressing in time, ω is then observed to decrease until it becomes negative again. This result indicates that, after an initial and temporary growth, any perturbation is always damped in the counterflow configuration as long as sufficient time has passed. In other words, sufficiently high applied strain rates (let us recall that case a500 of Table 1 does not reach a steady state) suppress the intrinsic instability onset, regardless of the initial perturbation wavelength. Note that the temporary positive growth rate region is relatively short, as it spans over a time up to $7\tau_f$.

Further insight on the role of strain rate in suppressing the intrinsic instabilities onset is provided next. By combining Eqs. (10) and (8), the growth rate can be rewritten as

$$\omega = \frac{1}{A}\frac{dA}{dk}\frac{dk}{dt} = -\frac{1}{A}\frac{dA}{dk}K_s k. \tag{11}$$

The above expression indicates that the growth rate in k space would vary linearly with the strain K_s if the derivative $\frac{dA}{dk}$ is independent of strain. To assess whether this is the case, one can compute the roots of k at zero growth rate, $k(\omega = 0)$. By looking at Eq. (11), since for the cases investigated K_s and k are always greater than zero, $\omega = 0$ only for $\frac{dA}{dk} = 0$. The values of k at zero growth rate, $k(\omega = 0)$, are plotted for the corresponding time $t(\omega = 0)$ in Fig. 9. At each initial perturbation λ_0 there corresponds a pair of $k(\omega = 0)$ points on the graph. Furthermore, two distinct sets of points can be identified. On the left-hand side, the 'earlier' roots of $\omega(k)$ are shown, which correspond to the points in Fig. 8 where the growth rate transitions in time from negative to positive. In contrast, the 'later' roots are located at the bottom-right, corresponding to the points in Fig. 8 where the growth rate shifts from positive to negative, ultimately suppressing the instabilities over time. The region enclosed by the iso-line (shaded in Fig. 9) represents the range of modes and times for which the growth rate is positive.

This figure highlights that the region of instability at the two higher strain rates, cases a2000 and a5000 of Table 1, almost perfectly overlap, while the same region of instability is broader at the lower strain rate case. In particular, the 'later' roots are closer to $k = 0$ in the a1000 case. This suggests that a further decrease of applied strain would virtually shift the values of $k(\omega = 0)$ at $k < 0$, meaning that there would not be any stabilisation over time. This is consistent with the discussion in the previous section, where an unsteady evolution of the flame front (which can be considered equivalent to a random perturbation) was observed for the relatively low strain case (case a500 of Table 1). In that case, in fact, strain is not sufficiently high and a succession of positive and negative growth rates occurs as time progresses, as shown by Fig. 4 where the amplitude of the local bumps in the flame front is observed to alternatively grow (due to intrinsic instabilities) and shrink (due to the stabilising effect of the flow field in the counterflow). As suggested by means of analytical analyses by Sivashinsky et al. [17] for stagnation point flames, a further decrease in strain levels is expected to result in growing instabilities similar to the unstretched premixed flame case. However, this instability would exhibit a non-linear onset due to the influence, albeit not dominant, of the tangential velocity component. Note that, although Sivashinsky et al. [17] analyse a different configuration, similar behaviours to those in the reactants-to-products setup can be expected at low strain, as the flame remains sufficiently distant from the wall or stagnation plane. However, at higher strain rates, stagnation point flame analyses may not be reliable due to unpredictable flame-wall interactions. For sufficiently high strain rates, instead, the observed growth rate pattern characterised by the shift of modes triggered by the tangential velocity becomes increasingly dominant over the single-mode constant growth rates typical of unstretched conditions, resulting in the stabilisation of the flame.

It is also worth noting that the collapse of the $\omega = 0$ iso-lines in the $k - at$ space for the two higher strain rate cases (a2000 and a5000) implies that the equation $\frac{dA}{dk} = 0$ is independent of strain in the limit of high applied strain rates. This suggests that $\omega(k)$ may become a linear function of K_s or a (recall Eq. (11)) in this limit. This consideration can be verified by looking at the growth rates normalised by the applied strain rate in Fig. 10. The figure shows that for the two higher strain rates, the curves overlap for the majority of the λ_0 cases, whereas no such overlap is observed for the lower strain rate case a1000. This observation confirms that at sufficiently high strain rate, the growth rate in k space becomes a linear function of strain rate itself, with the derivative $\frac{dA}{dk}$ becoming independent on K_s or a. Hence, for a given initial perturbation λ_0, a characteristic $\omega(k)$ proportional to the applied strain rate can be identified in the counterflow configuration.

To understand the physics behind this phenomenon, it is convenient to define two distinct time scales. The rate of change of the wavelength due to the counterflow characteristic velocity in y-direction, $\frac{d\lambda}{dt}$, defines a mode-shifting time scale, τ_{MS}. Meanwhile, τ_{DR} represents the time required for a given mode to adapt its growth rate to its characteristic unstretched dispersion relation $\omega(k)$. At high strain levels $\frac{d\lambda}{dt}$ is very high and determines a τ_{MS} that is much shorter than τ_{DR}. This implies that before a perturbation can be affected by the characteristic $\omega(k)$ at unstretched conditions, it has already transitioned to another mode, and $\omega(k)$ will thus follow a characteristic pattern uniquely defined by the counterflow configuration at the given λ_0 and applied strain rate. In the a1000 case, instead, $\frac{d\lambda}{dt}$ is still low enough to allow the unstretched characteristic $\omega(k)$ to partially sum up to the characteristic counterflow growth rate and ultimately affect the total $\omega(k)$, triggering overall higher transient growth rates in the region of instability. Note that, for the two lowest λ_0 cases, one can observe a non-perfect scaling also for the a2000 case when $k \gtrsim 1500$ m^{-1}. This can be explained by the fact that, at earlier times, smaller initial perturbations exhibit lower values of $\frac{d\lambda}{dt}$ compared to wider initial perturbations (see Fig. 7(a)), resulting in a larger τ_{MS} even at higher strain rates.

Overall, the analysis carried in the present study shows that from moderate strain rate upwards, intrinsic instabilities are always damped after sufficient time in a counterflow configuration. At further increased strain rates, the transient shape of $\omega(k)$ becomes completely unaffected by the characteristic growth rate of each mode in unstretched conditions, and is uniquely determined by the applied strain rate and the initial imposed perturbation wavelength.

4. Conclusions

Detailed chemistry, two-dimensional simulations have been conducted on pure hydrogen lean premixed flames in counterflow configuration at different strain rates. The response of the flame to ranging wavelengths perturbations has been assessed and the following regimes can be identified considering the onset of intrinsic instabilities:

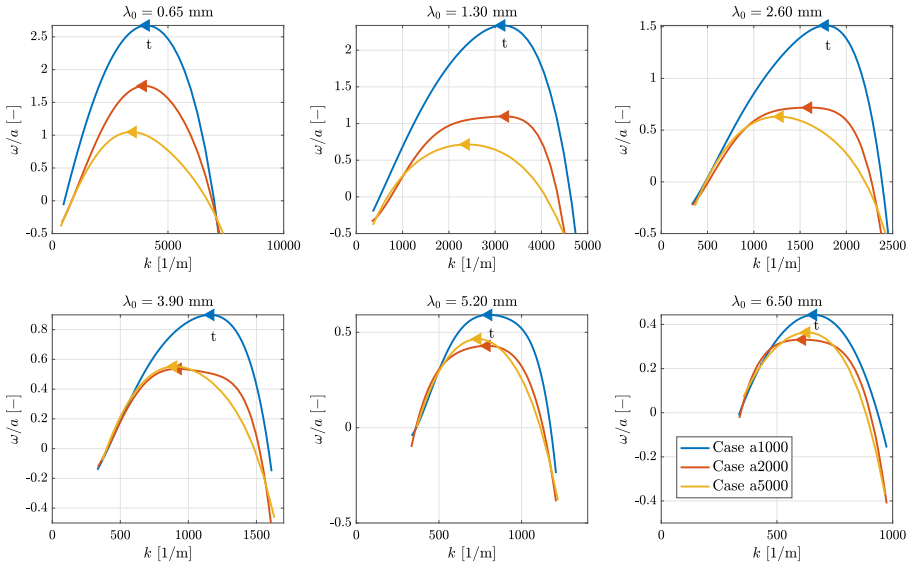

Fig. 10. Growth rate ω as a function of the wave number k normalised by the applied strain rate a at different initial perturbation wavelengths λ_0.

- At very low strain rates, the mode shift time scale is greater than the dispersion relation time scale ($\tau_{MS} > \tau_{DR}$). As suggested analytically by Sivashinsky et al. [17] for stagnation point flames, intrinsic instabilities always grow similarly to an unstretched premixed flame case at the same conditions, because the perturbation has enough time at a given mode to be strongly influenced by the destabilising growth rate of the dispersion relation $\omega_{DR}(k)$. However, ω would still follow a non-linear onset due to the counterflow-characteristic presence, albeit not dominant, of a flame-tangential velocity component triggering a slow mode shifting.
- At low to moderate strain rates, the mode shift time scale is comparable to the dispersion relation time scale $\tau_{MS} \approx \tau_{DR}$. Here, the intrinsic instabilities onset triggered by the destabilising growth rates from the unstretched dispersion relation and the stabilising effect of the mode shifting in the counterflow define an unstable equilibrium, where a sequential pattern is established featuring first a growth and then a damping of the perturbation.
- At moderate to high strain rates, the mode shift time scale is smaller than the dispersion relation time scale $\tau_{MS} < \tau_{DR}$. From this level of strain onward, any forced perturbation is damped after sufficient time, as the perturbation switches from a mode to another before the mode has time to adapt its growth rate to the one of the unstretched dispersion relation. Nevertheless, ω_{DR} maintains a mild destabilising influence on the growth rate in k space, such that $\omega(k)$ is not yet a linear function of strain.
- at high to very high strain rates, the mode shift time scale is much smaller than the dispersion relation time scale $\tau_{MS} \ll \tau_{DR}$. Here, not only any perturbation is always damped after sufficient time, but also the transitory growth rate evolution is independent on ω_{DR}, establishing a pattern that is uniquely defined by the perturbation wavelength and linearly dependent on the applied strain rate.

Overall, this study demonstrates for the first time using high-fidelity numerical simulations that intrinsic instabilities in a counterflow configuration are suppressed by sufficiently high applied strain rates, following a transient onset uniquely defined by both the initial perturbation and the applied strain itself.

Future works will aim to extend this analysis to three-dimensional laminar and turbulent counterflow cases, laying the groundwork for stabilising lean premixed hydrogen flames in strained configurations in practical combustion systems.

Novelty and significance statement

The novelties of this study are summarised below:

- This study conducts an extensive exploration of the onset of intrinsic flame instabilities in lean hydrogen/air premixed flames within a strained counterflow setup for the first time, employing high-fidelity numerical simulations.
- Unlike intrinsically unstable lean premixed hydrogen/air unstretched flames, this study promisingly finds that thermodiffusive instabilities are suppressed by sufficiently high strain rate in a counterflow configuration.
- This study demonstrates that the onset of intrinsic flame instabilities in a counterflow configuration at high strain rate follow a transient onset uniquely defined by both the initial perturbation and the applied strain.

CRediT authorship contribution statement

Alessandro Porcarelli: Writing – original draft, Visualization, Validation, Software, Investigation, Funding acquisition, Formal analysis, Data curation, Conceptualization. **Pasquale Eduardo Lapenna:** Writing – review & editing, Supervision, Methodology, Formal analysis, Conceptualization. **Francesco Creta:** Writing – review & editing, Supervision, Methodology, Formal analysis, Conceptualization. **Ivan Langella:** Writing – review & editing, Project administration, Funding acquisition, Conceptualization.

Declaration of competing interest

The authors declare that they have no known competing financial interests or personal relationships that could have appeared to influence the work reported in this paper.

Acknowledgements

AP and IL acknowledge the Dutch Ministry of Education and Science for providing project funding support via the Sector Plan scheme. AP further acknowledges financial support to perform Short Term Scientific Mission (STSM) at Sapienza (Rome) from the CYPHER consortium (COST ACTION CA22151). IL further gratefully acknowledges financial

support from the ERC Starting Grant OTHERWISE, grant n. 101078821. PEL and FC acknowledge financial support by ICSC (Centro Nazionale di Ricerca in HPC, Big Data and Quantum Computing) funded by the European Union – NextGenerationEU. The authors also acknowledge the use of the Dutch National Supercomputer Snellius grant EINF-10039 to perform the simulations.

Appendix A. Supplementary data

Supplementary material related to this article can be found online at https://doi.org/10.1016/j.proci.2025.105906.

References

[1] E.-S. Cho, S.H. Chung, Improvement of flame stability and NOx reduction in hydrogen-added ultra lean premixed combustion, J. Mech. Sci. Technol. 23 (3) (2009) 650–658.
[2] P.E. Lapenna, L. Berger, F. Creta, H. Pitsch, Hydrogen laminar flames, in: Hydrogen for Future Thermal Engines, Springer, 2023, pp. 93–139.
[3] M. Matalon, B.J. Matkowsky, Flames as gasdynamic discontinuities, J. Fluid Mech. 124 (1982) 239–259.
[4] G. Sivashinsky, Diffusional-thermal theory of cellular flames, Combust. Sci. Technol. 15 (3–4) (1977) 137–145.
[5] F. Creta, M. Matalon, Strain rate effects on the nonlinear development of hydrodynamically unstable flames, Proc. Combust. Inst. 33 (1) (2011) 1087–1094.
[6] C.E. Frouzakis, N. Fogla, A.G. Tomboulides, C. Altantzis, M. Matalon, Numerical study of unstable hydrogen/air flames: shape and propagation speed, Proc. Combust. Inst. 35 (1) (2015) 1087–1095.
[7] L. Berger, A. Attili, H. Pitsch, Intrinsic instabilities in premixed hydrogen flames: Parametric variation of pressure, equivalence ratio, and temperature. part 1-dispersion relations in the linear regime, Combust. Flame 240 (2022) 111935.
[8] S. Al Kassar, L. Berger, P.E. Lapenna, F. Creta, H. Pitsch, A. Attili, Efficient and accurate calculation of dispersion relations for intrinsically unstable premixed flames, Combust. Flame 269 (2024) 113640.
[9] P.E. Lapenna, A. Remiddi, D. Molinaro, G. Indelicato, F. Creta, A-posteriori analysis of a data-driven filtered wrinkled flamelet model for thermodiffusively unstable premixed flames, Combust. Flame 259 (2024) 113126.
[10] A. Remiddi, P.E. Lapenna, D. Cavalieri, D. Schintu, G. Indelicato, A. Attili, L. Berger, H. Pitsch, F. Creta, Data-driven modeling of resolved and filtered thermo-diffusively unstable hydrogen–air flames, Proc. Combust. Inst. 40 (1–4) (2024) 105713.
[11] L. Berger, A. Attili, H. Pitsch, Synergistic interactions of thermodiffusive instabilities and turbulence in lean hydrogen flames, Combust. Flame 244 (2022) 112254.
[12] P.E. Lapenna, G. Troiani, F. D'Alessio, F. Creta, Synergistic interplay of thermod-iffusive instability and turbulence in premixed flames, Proc. Combust. Inst. 40 (1–4) (2024) 105499.
[13] J. Van Oijen, A. Donini, R. Bastiaans, J. ten Thije Boonkkamp, L. De Goey, State-of-the-art in premixed combustion modeling using flamelet generated manifolds, Prog. Energy Combust. Sci. 57 (2016) 30–74.
[14] A. Porcarelli, B. Kruljević, I. Langella, Suppression of NOx emissions by intensive strain in lean premixed hydrogen flamelets, Int. J. Hydrog. Energy (2023).
[15] A. Porcarelli, I. Langella, Mitigation of preferential diffusion effects by intensive strain in lean premixed hydrogen flamelets, Proc. Combust. Inst. 40 (1–4) (2024) 105728.
[16] L. Berger, A. Attili, M. Gauding, H. Pitsch, Effects of Karlovitz number variations on thermodiffusive instabilities in lean turbulent hydrogen jet flames, Proc. Combust. Inst. 40 (1–4) (2024) 105219.
[17] G.I. Sivashinsky, C.K. Law, G. Joulin, On stability of premixed flames in stagnation-point flow, Combust. Sci. Technol. 28 (3–4) (1982) 155–159.
[18] T. Poinsot, D. Veynante, Theoretical and Numerical Combustion, RT Edwards, Inc., 2005.
[19] Eindhoven University of Technology, CHEM1D. A one dimensional laminar flame code, 2021.
[20] J.O. Hirschfelder, C.F. Curtiss, R.B. Bird, The Molecular Theory of Gases and Liquids, John Wiley & Sons, 1964.
[21] A.J. Fillo, J. Schlup, G. Blanquart, K.E. Niemeyer, Assessing the impact of multi-component diffusion in direct numerical simulations of premixed, high-Karlovitz, turbulent flames, Combust. Flame 223 (2021) 216–229.
[22] B. Naud, M. Arias-Zugasti, A. Cuoci, Complete multicomponent versus mixture-averaged calculations of a laminar H2/N2 diffusion flame including heat transfer at the burner and Soret effects, Int. J. Hydrog. Energy (2025).
[23] L. Berger, A. Attili, H. Pitsch, Intrinsic instabilities in premixed hydrogen flames: parametric variation of pressure, equivalence ratio, and temperature. Part 2–Non-linear regime and flame speed enhancement, Combust. Flame 240 (2022) 111936.
[24] A. Evlampiev, Numerical Combustion Modeling for Complex Reaction Systems (Ph.D. thesis), Technische Universiteit Eindhoven, 2007.
[25] M. Ó Conaire, H.J. Curran, J.M. Simmie, W.J. Pitz, C.K. Westbrook, A comprehensive modeling study of hydrogen oxidation, Int. J. Chem. Kinet. 36 (11) (2004) 603–622.